Molecular BioSystems

Accepted Manuscript

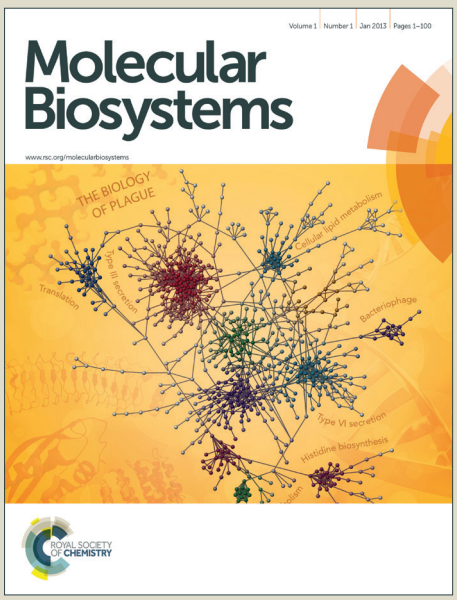

ROYAL SOCIETY OF CHEMISTRY

www.rsc.org/molecularbiosystems

Journal Name

RSCPublishing

ARTICLE

Sequence Context Induced Antimicrobial Activity: Insight to Lipopolysaccharide Permeabilization

Anirban Ghosh,[a,Ψ] Aritreyee Datta,[a,Ψ] Jagannath Jana,[a,Ψ] Rajiv K. Kar,[a] Chiradip Chatterjee,[b] Subhrangsu Chatterjee[a,*] and Anirban Bhunia[a,*]

Cite this: DOI: 10.1039/x0xx00000x

Received 00th January 2012,
Accepted 00th January 2012

DOI: 10.1039/x0xx00000x

www.rsc.org/

Lactoferrampin (WR17, Trp 268-Arg 284), an antimicrobial peptide is known to have significant antibacterial and candidacial activity. However, there were no previous studies explaining how WR17 permeabilizes the outer membrane of gram negative bacteria and neutralizes endotoxins. In this study we used a series of assays like antimicrobial activity, calcein leakage, NPN dye uptake and endotoxin neutralization assay to show that the sequence context of WR17 modulates its multi-faceted activities. We determined the high resolution NMR structure of WR17 in LPS and found that the N-ter region forms a helix (Trp1-Phe11) and orients itself at an angle of 45° into the lipopolysaccharide (LPS) micelle, whereas, the C-ter region (Lys13-Arg17) remains as a flexible extended random coil. We also verified this result through *in-silico* molecular modeling simulation. Isothermal titration calorimetry showed that the interaction of WR17 and its analogues with LPS was primarily endothermic in nature. Using several fluorescence techniques such as anisotropy and red edge excitation shift assay we revealed a motional restriction for Trp1 of WR17 in LPS. The distance between an indole ring of Trp1 of WR17 and the polar head group of LPS is around 7 Å, as obtained from the depth of insertion assay. Additionally, MD simulation demonstrated that the incorporation of the peptide in LPS is achieved by the help of $K^{13}xK^{15}xR^{17}$ motif at the C-terminus. This novel anchoring "$K^{13}NKSR^{17}$" motif is currently being utilized in our ongoing research to design novel anti-endotoxic molecules.

Introduction

Lipopolysaccharide (LPS), a glycolipid component present in the outer leaflet of the outer membrane of gram negative bacteria plays a pivotal role in bacterial infections affecting human health.[1] LPS presents itself as an impermeable barrier in bacterial membrane, protecting them from a hoard of antibacterial agents and subsequently contribute to septicemia or endotoxic shock in human and animals.[2] A study conducted in the United States alone showed a steady rise in deaths associated with sepsis reaching a striking annual average mortality rate of 120,000.[3] Sepsis, due to gram negative bacterial infections is caused by a hyper activated innate immune response leading to excessive production of TNFα and other immune-modulatory cytokines which leads to severe damage to tissue and organs. This phenomenon leads to a steep fall in blood pressure and associated multiple organ failure and coagulopathy.[4] LPS, the key bio-molecule in sepsis through its immune-modulatory effects, mediates the hyperactive immune response through a cascade of signalling pathways.[5-7] Initially, LPS is released into blood upon lysis of the bacterial cell wall and binds to LPS binding protein (LBP). Next, is carried to CD14 receptors present on the surface of immune cell membrane. CD14 takes LPS to *myeloid differentiation protein-2* (MD2) that is associated to toll like receptor protein, TLR4. TLR4, upon binding to LPS activates the signalling cascade responsible for the cytokine burst which includes TNFα, IL-6, IL-8 and IL-1.[8-10] Thus LPS establishes itself as a prime target for pharmacological intervention towards development of effective antibacterial and anti-sepsis drug.

The current rise in multi-drug resistant bacteria has been a threat to human health, developing itself into a grave concern seeking urgent solution. Many of the pathogenic gram negative bacterial strains like *Pseudomonas aeruginosa*, *Klebsiella pneumoniae* etc. have developed resistance against a variety of antibiotics rendering their bactericidal activity totally ineffective.[1, 11] Agents which can sequester and/or neutralize LPS would prove to be an invaluable therapeutic candidate.[12] In this context, cationic antimicrobial peptides (AMPs) which can lyse the bacterial membrane are being extensively studied from the structure-function point of view, to gain insights into their mechanism of action. AMPs have been studied for a long time as a potential alternative to the conventional antibiotics due to their significant prevalence in nature and generalized mode of action, against micro-organisms that make pathogen adaption to resistance difficult.[13, 14] AMPs have been implicated in the innate immune response of plants and animals and play a vital role in acting as the first line of defence against invading pathogens.[15,16] AMPs are are rich in basic non-polar residues and their amphipathic nature is evolutionarily conserved.[16-18] They exhibit diverse structures and fold to adopt unique conformational topologies upon interaction with their target.[19] It is noteworthy to mention that the amphipathic nature of these molecules allows them to interact with both the inner and outer membranes of bacteria, leading to membrane disintegration.[20, 21] In addition, many of these AMPs have also been found to be endowed with endotoxin neutralization abilities.[16, 18] Due to the diversity noted in the structures of these naturally occurring AMPs no general characterization is possible with regard to their mechanism of action. Hence, each one of them needs to be studied individually to define the specific residues responsible for imparting antimicrobial and anti-endotoxic activities.[22]

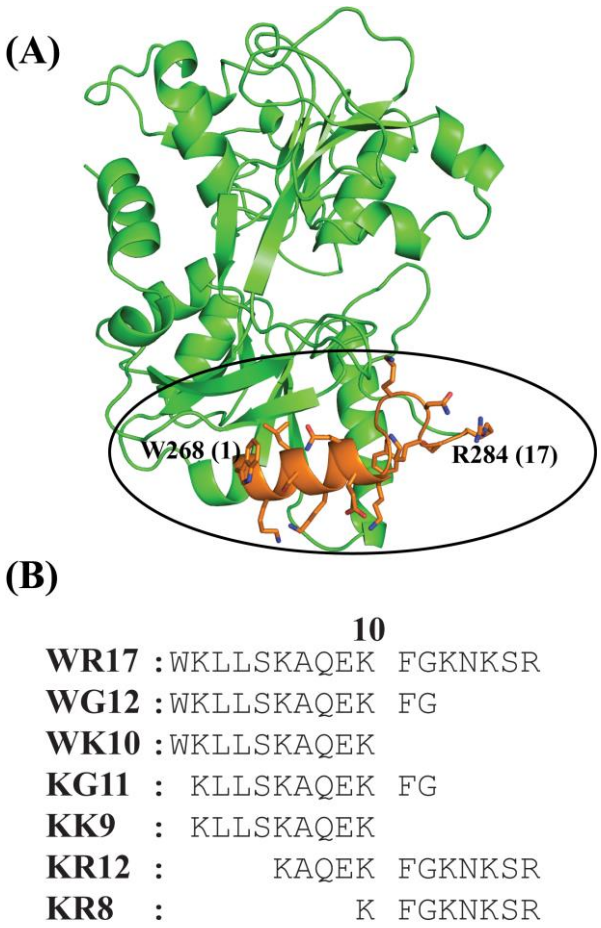

Fig. 1. Cartoon diagram of bovine lactoferrin and amino acid sequences of WR17 and its shorter fragments. (A) Ribbon diagram of bovine lactoferrin (Protein Data Bank accession code 1BLF) and a 17 residue antimicrobial peptide in an N1 - domain has been denoted as lactoferrampin (WR17, amino acids Trp268–Arg284) which is marked with a black circle. The figure was prepared using Pymol. (B) Amino acid sequence of WR17 and its N- and C-ter truncated peptides WG12, WK10, KG11, KK9, KR12 and KR8 analogue.

In the present study, the interaction of bovine lactoferrin (Trp268-Arg284, hereafter denoted as WR17) (Fig 1A) with LPS using various biophysical techniques like Circular Dichroism, fluorescence, isothermal titration calorimetry (ITC), dynamic light scattering and high resolution NMR spectroscopy in conjunction with MD simulation was performed to provide structural insights into its mechanism of action. Further, we decided to investigate the structure-activity relationships by designing shorter peptide analogues from WR17, based on its sequence (Fig. 1B) in order to obtain residue-specific information. At the outset, the spectroscopic study yields not only the details of binding phenomenon, but also hints at the importance of the residues responsible for its noted activity.

Results and discussion

Designing of peptides

The three-dimensional structure of the protein, lactoferrin, consists of several α-helices, β-sheets and β-turn or loop (Figure 1A).[23] Lactoferricin B of residues 17-41 adopts twisted β-sheet structure Similar to other AMPs including magainin or cecropin, the N-ter part of lactoferrampin (residues 268-284) peptide adopts an amphipathic α-helical conformation upon binding to membranes like dodecaphosphocholine (DPC) or sodium dodecyl sulfate (SDS).[24] The three-dimensional solution structure of lactoferrampin (WR17) (Figure 1A) or its

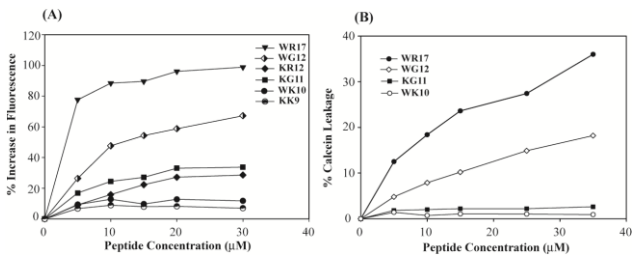

Fig. 2. Permeabilization of outer-membrane and vesicle leakage from the model membrane by WR17 and its fragments. (A) Plot shows extent of permeabilisation of *E. coli* BL21 in the form of the percentage increase of fluorescence of NPN dye plotted against increasing concentrations of WR17 and its fragments WG12, KR12, KG11, WK10 and KK9. A significant reduction in the amount of permeabilization is observed in case of fragments of WR17 when compared to itself showing that they have a reduced ability to induce outer membrane permeabilization. (B) The plot shows the efficiency of calcein dye leakage from small unilamellar vesicles (SUV) composed of 3:1 POPC:POPG lipids in percentage of leakage as a function of the concentrations of peptides. The 0.1% Triton X 100 has been used as a control to obtain maximal leakage using which percentage of leakage of the peptides has been calculated (see experimental section for equation).

analogues including longer version of lactoferrampin (residues 265-284) in the presence of per-deuterated lipid micelles such as zwitter-ionic DPC or negatively charged SDS clearly shows that the N-ter part of WR17 (residues Trp1-Phe11) adopts an α-helical conformation while the final 6-residues, Gly12-Arg17, at the C-terminus region remains unstructured.[24] The flexible C-ter end of WR17 is cationic in nature and is vital for antibacterial activity of the peptide. Structurally, the aromatic ring of Phe11 orients itself in the same plane as that of the indole ring of Trp1 which serves as an anchor for the lipid bilayer.[25, 26] Solid-state NMR experiment in conjunction with MD simulation confirms the tilt angle of the N-ter helix to be 45° with respect to the bilayer, which in turn facilitates the penetration of the peptide into the lipid bilayer.[27] Several other biophysical techniques such as fluorescence, differential scanning calorimetry (DSC) etc. were used to understand the mechanism of action of this peptide and its analogues in multilamellar vesicles.[22, 24, 28] However, it is necessary to understand the high resolution structure of this peptide in the context of LPS because the AMPs interact with the outer membrane components first before gaining access to the inner membrane.[29, 30]

Here, we have chosen WR17 of lactoferrin to understand the structure-function correlation using high resolution NMR spectroscopy. Since Trp has a distinct preference to bind to the membrane interface so we truncated it to WG12, to investigate the role of the aromatic amino acids in LPS binding. The individual roles of Trp or Phe in WR17 were deduced by designing peptides containing either Trp (WK10) alone or Phe alone (KG11) or both (WG12). A negative control peptide, KK9, with both the aromatic amino acid residues removed has also been adopted in this study. The importance of Lys and Arg rich C-ter region was judged by truncating the fragments into KR8 and KR12 (Fig 1B).

Antimicrobial activity assay

We studied the antimicrobial activity of WR17 and its truncated analogues against gram negative *P. aeruginosa ATCC 27853, Xanthomonas campestris pv campestris* and gram positive *Bacillus subtilis*. WR17 inhibited *P. aeruginosa, X.campestris* and *B.subtilis* at 9.5, 10 and 20 µM, respectively (Table S1). On the other hand, among the truncated analogues, only WG12 (deletion of five residues from C-ter) showed antimicrobial activity against *X. campestris* at 75 µM. All the other analogues showed no activity against any of the pathogens tested. This result indicates that C-terminal positively charged residues also play an important role for antimicrobial activity of the parent peptide to make it more potent in comparison to others.

Outer Membrane permeabilization assay through NPN dye uptake

Primarily, we wanted to understand whether WR17 or its analogues can permeabilize the *E.coli* cells, using 1-N-phenylnaphthylamine (NPN) dye uptake assay. The disruption of the outer membrane by the treatment with AMPs allows the dye to enter into the bacterial cytoplasmic membrane resulting in an enhanced emission of fluorescence intensity. As shown in Fig 2A, WR17 showed a dramatic increase in the emission intensity of NPN by ~ 98 % at a concentraion of 30 µM. Surprisingly, WG12, KG11 and KR12 could achieve only a maximum fluorescence of 67 %, 35 % and 28 %, respectively at the similar concentration of each peptide. WK10 and KK9 showed a negligible fluorescence intensity enhancement of only 15 % (Fig. 2A). These results indicate that WR17 is capable of disrupting the intact outer membrane model efficiently. Nonetheless, its N- and C-ter fragments alone are incapable of permeabilizing the cell membrane with only WG12 showing partial activity. Thus, it may be possible that Trp1 and Phe11 are crucial for the outer membrane permeabilizing activity of the intact peptide WR17.

Calcein leakage assay

In the next attempt, to determine the vesicle leakge from the model membrane by native WR17 and its fragments WG12, KG11, WK10, KR12, KR8 and KK9 calcein dye leakage assay using POPC: POPG (3:1 molar ratio) lipid vesicles was performed.[31, 32] The fluorescence intensity of calcein increases, due to release of the dye from the lipid vesicle upon disruption caused by addition of the peptide. Native peptide WR17 showed a 36 % increase in the fluorescence intensity as shown in Fig. 2B. In comparison, the calcein leakage activity for WG12 was reduced to half of WR17. Peptide fragments WK10 and KG11 showed negligible activity, whereas KR12, KR8 and KK9 showed no dye leakage.

Neutralization of endotoxin

Limulus amoebocyte lysate (LAL) assay is an extremely useful assay to identify the inhibition and neutralization activity of LPS with a sensitivity as low as pico-molar. The experiment was carried out at three different LPS/endotoxin concentrations of 0.25, 0.5 and 1 EU/ml with six different peptide concentrations of 5, 10, 15, 25, 50 and 100 µM. It was observed that WR17 was capable of neutralizing 0.25 EU/ml at a concentration of 5 µM and 1 EU/ml at a concentration of 15 µM (Table S2). On the other hand, similar endotoxin concentrations of 0.25 EU/ml and 1 EU/ml were neutralized by

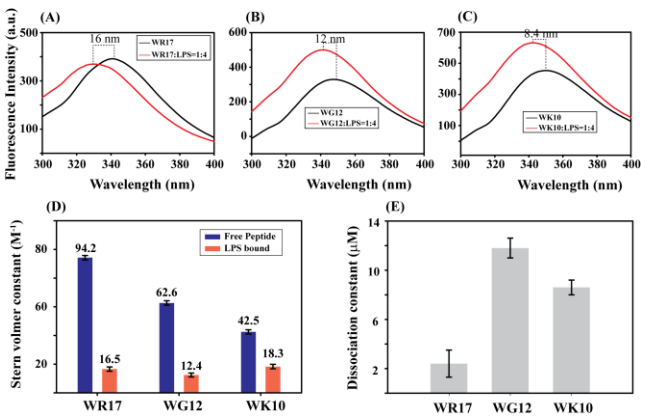

Fig.3. Different fluorescence experiments showing binding affinity and solvent accessibility of peptides towards LPS. (Upper panel) Intrinsic Tryptophan fluorescence emission spectrum of (A) WR17, (B) WG12 and (C) WK10, respectively in the presence of LPS at a molar ratio of 1:4. (D) Bar diagram showing Stern-Volmer constant of the mentioned peptides in aqueous as well as in the presence of LPS. (E) Bar diagram demonstrating equilibrium dissociation constant (K_D) of the peptides in LPS bound state derived using following changes in emission maxima with LPS concentrations. All fluorescence experiments were performed in 10 mM sodium phosphate buffer (pH 6.0) at 298 K.

WG12 at 25 μM and 50 μM, respectively. All the other fragments were unable to neutralize the endotoxin.

Interaction study using Fluorescence Spectroscopy and ITC

The presence of Trp residue in the peptides WR17, WG12 and WK10 was used to determine the binding parameters. Generally, the change in the fluorescence emission maxima (λ_{max}) of Trp is used as a sensitive probe to monitor the

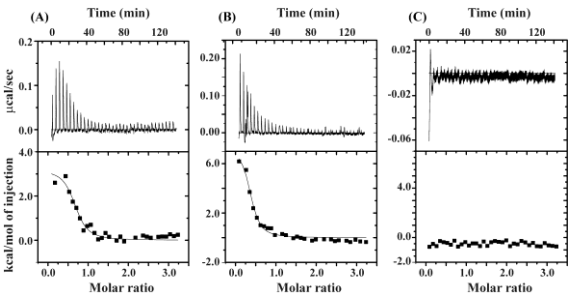

Fig. 4. Isothermal titration Calorimetric (ITC) profile for WR17, WG12 and KK9. The upper panel shows the endothermic heat of reaction vs. time (minute) upon interaction with LPS for peptides (A) WR17, (B) WG12 and (C) KK9, respectively. The lower panel of the figures A, B and C shows enthalpy change per mole of peptide injection vs. molar ratio (peptide:LPS) for peptides WR17, WG12 and KK9 respectively upon interaction with LPS. 10 μM of LPS were titrated against 250 μM of peptides. All peptides and LPS were dissolved in 10 mM phosphate buffer at pH 6.0.

interaction of the ligand with a macromolecule. The Trp residue of WR17, WG12 and WK10 in free solution showed an emission maximum at ~ 350 nm, which argues that the Trp residue is exposed to the aqueous environment (Fig. 3A-C). However, the successive addition of LPS into the peptide solution at an increasing molar ratio yielded a progressive blue shift of the emission maxima. The blue shift observed for the Trp residue of WR17/WG12/WK10 in the presence of LPS indicates the presence of Trp in the hydrophobic or non-polar environment (Fig. 3A-C). The extent of blue shift was highest for WR17 with a shift of 16 nm, whereas its analogues, WG12 and WK10 recorded a blue shift of about 12 and 8.4 nm, respectively. The larger blue shift of the emission wavelength provides evidence for the deep insertion of the Trp residue of WR17 in the hydrophobic environment of LPS compared to that of the analogues WG12 and WK10. Therefore, the extent of the solvent exposure of Trp residues in WR17/WG12/WK10 was further investigated by means of static quenching with a neutral quencher acrylamide in free solution as well as in complex with LPS. All of the peptides exhibited much higher Stern-Volmer Quenching Constants (K_{SV}) in free-state compared to the LPS bound state indicating that the Trp residue is well embedded inside the LPS which protects its accessibility to the quencher (Fig. 3D). This quenching data is in good agreement with the fact that the Trp has an indiscriminate preference for the interfacial region of the lipid bilayer.[25] Additionally, the changes of fluorescence emission maxima of Trp in

Table 1. Thermodynamic parameters derived from ITC experiment.

Parameters	WR17	WG12
K_A (μM^{-1})	2.6	2.2
ΔH (kcal.mol^{-1})	3.2 ± 0.4	6.3 ±
$T\Delta S$ (kcal.mol^{-1})	11.9	14.9
ΔG (kcal.mol^{-1})	-8.7	-8.6
K_D (μM)	0.4	0.5

WR17/WG12/WK10 in the presence of LPS yielded an equilibrium dissociation constant (K_D) of 2.4 ± 0.1, 11.8 ± 0.3 and 8.6 ± 0.6 μM, respectively (Fig. 3E). Altogether, the larger blue shift and lower K_D values observed in case of WR17 is attributed to the strong electrostatic interaction between the positively charged residues, Lys and Arg at the C-ter region of WR17 and the negatively charged phosphate head group of LPS. Due to the lack of Trp residues in the analogues KG11, KK9, KR12 and KR8, the fluorescence based assays in the presence of LPS could not be carried out. To determine the depth of insertion of Trp into the LPS bilayer fluorescence-quenching studies were carried out using two spin-labeled lipids, 5-DSA and 16-DSA. The position of Trp residues from the center of the LPS player for WR17 and WG12 was found to be around 7.4 and 7.1 Å, respectively (Table S2). This distance information indicates that the Trp residue of both the peptides is well inserted in the LPS bilayer and forms strong van-der-

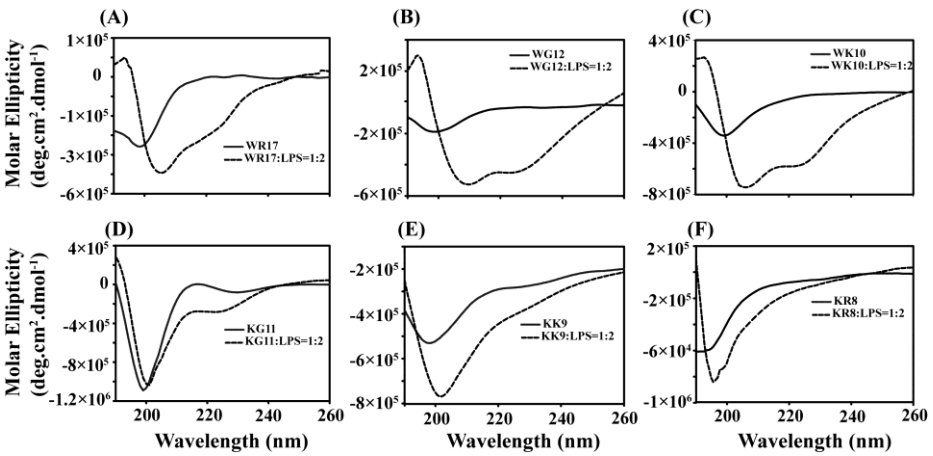

Fig. 5. Secondary structures of peptides in free and LPS bound forms by Circular Dichromism. Far-UV CD spectra of native WR17 (A), WG12 (B), and WK10 (C) (solid panel), KG11 (D), KK9 (E) and KR8 (F) (lower panel) in the absence (dashed line) and the presence of *E. coli* 0111:B4 LPS (red line). All CD spectra were performed in 10 mM sodium phosphate buffer (pH 6.0) at 298 K.

Waals interaction with the acyl chains of LPS (Table S3).

Additionally, isothermal titration calorimetry (ITC) experiments were performed to obtain the equilibrium dissociation constant (K_D) and the binding energy of the active peptides WR17 and WG12 with LPS (Fig. 4). As a control experiment the binding interaction of the inactive KK9 (peptide

without Trp1 and Phe11) with LPS was also performed. It is noteworthy to mention that KK9 can neither penetrate the outer-membrane of the cell nor bacterial inner membrane (Fig. 2). The binding of WR17-LPS or WG12-LPS is a spontaneous, entropy driven process (ΔG=-8.7 kcal mol^{-1}) with a dissociation constant (K_D) of about 0.4 and 0.5 μM, respectively (Table 1). This data corroborates well with other AMP-LPS based studies performed by ITC, where it was reported that the interaction is strongly entropy driven and has an upward ITC profile.[33, 34] As predicted, KK9 did not show any binding to the LPS micelle (Fig. 4C).

Secondary structure of peptides in LPS

Fig. 5 shows the far UV CD spectra of the peptides WR17, WG12, WK10, KG11, KK9 and KR12/KR8 in the absence and presence of LPS, respectively. In the aqueous solution, native WR17 as well as its C- and N-ter truncated analogues (Fig. 1) showed a strong negative band at 200 nm, indicating that the free peptides adopt a disordered or random-coil conformation. LPS induces a drastic change in the CD spectra of native WR17, WG12 and WK10. The negative CD ellipticity at ~ 200 nm observed for the free peptides disappeared upon addition of LPS, with a concomitant increase in the intensity of a positive peak at ~195 nm and two negative peaks with maxima centering at ~ 208 nm and at ~ 222 nm. This demonstrates formation of alpha-helical conformation of these peptides in LPS micelle (Fig. 5A-C). Interestingly, the minima observed at ~ 222 nm for WR17 in the presence of LPS is broadened, signifies the greater extent of the dynamics taking place in some part of the alpha helical region. On the contrary, the WG12 peptide in LPS micelle showed two minima at ~ 208 and ~ 222 nm with equivalent intensities. WK10 formed by removing Phe11 and Gly12 residues at the C-ter region of WG12, showed a partial loss in the helical structure, in the presence of LPS micelle. Other analogues, KG11, KK9 and KR8 in the presence of LPS did not show any significant changes in the secondary structure (Fig. 5D-F). Moreover, the slight changes in the intensity near the negative maxima around ~ 200 nm for KK9 and KR8 can be attributed to the electrostatic interaction between the positively charged side chains of the terminal amino acids and negatively charged phosphate groups of the LPS moiety. Overall the CD data identifies the structural changes taking place in the parent and the truncated analogues of WR17 upon binding to LPS.

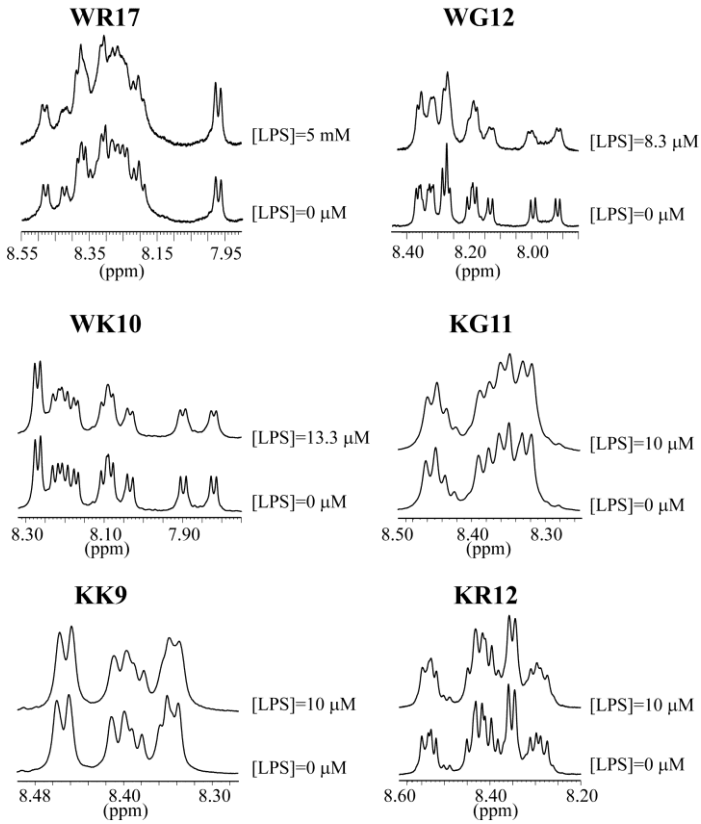

Fig. 6. Interaction of peptides with LPS by NMR. One-dimensional amide proton resonance NMR spectra of WR17 and its analogues.

NMR Studies of Peptides in free LPS Micelle

One dimensional ^{1}H NMR spectra of WR17 and its N-ter analogues, WG12 and WK10 as well as the C-ter analogues, KR12 or KR8 show a large dispersion for the amide proton resonances (7.7 – 8.6 ppm) (Fig. 6). In contrast, the control peptides, KG11 or KK9 showed a severe signal overlap in the one-dimensional ^{1}H NMR spectra, suggesting a random coil conformation for the peptide. Interestingly, addition of LPS even at a low concentration of ~ 5-20 μM to the sample containing the peptides (~ 1 mM) showed extensive line-shape broadening in the proton dimension for WR17, WG12, WK10 and KR12 without causing any chemical shift perturbation (Fig. 6). This result is a clear evidence of the peptide undergoing conformational exchange between the free and the LPS bound form, in the fast to intermediate time scale.[35] In addition to the line broadening effect seen for the amide protons of WR17/WG12/WK10, the most downfield resonances of the indole ring protons ($N^{\varepsilon}H$) of Trp also showed a substantial line broadening effect (data not shown). Further, three-dimensional structures of all the peptides in the presence of LPS was carried out using *transferred* Nuclear Overhauser effect spectroscopy (*tr*NOESY) experiments.[34, 36] *tr*NOESY is an extremely useful technique to determine the three-dimensional structure of the ligands bound to the macromolecule when the chemical exchange between the free and the bound state falls within the fast to intermediate regimes, with a dissociation constant (K_D) in the range of micro-molar to milli-molar.[37] The complete sequence specific proton resonance assignments for all the free peptides in solution were determined with the help of both two-dimensional total correlation spectroscopy (TOCSY) and NOESY.[38] The NOESY spectra for all the peptides showed only a weak intra- and sequential NOE between the backbone and side chain proton resonances. In addition, the aromatic amino acid residues such as Trp1 and Phe11 did not show any notable NOE between the side chain of the hydrophobic amino acids and their aromatic ring protons (ESI Fig. S1). The lack of NOEs indicates that the peptides are highly flexible in solution and do not adopt any folded conformation. This result is in good agreement with the CD spectra, where we demonstrated that all the peptides considered here adopts random coil or unstructured conformation.

On the other hand, addition of LPS even in small quantity to WR17, WG12 and WK10 showed a marked increase in the number of NOEs, owing to the fact that peptide adopts a folded conformation in presence of LPS**.** As LPS forms a high molecular weight micelle even at a very low concentration (<1 μM), the peptide that interacts with this large LPS micelle also

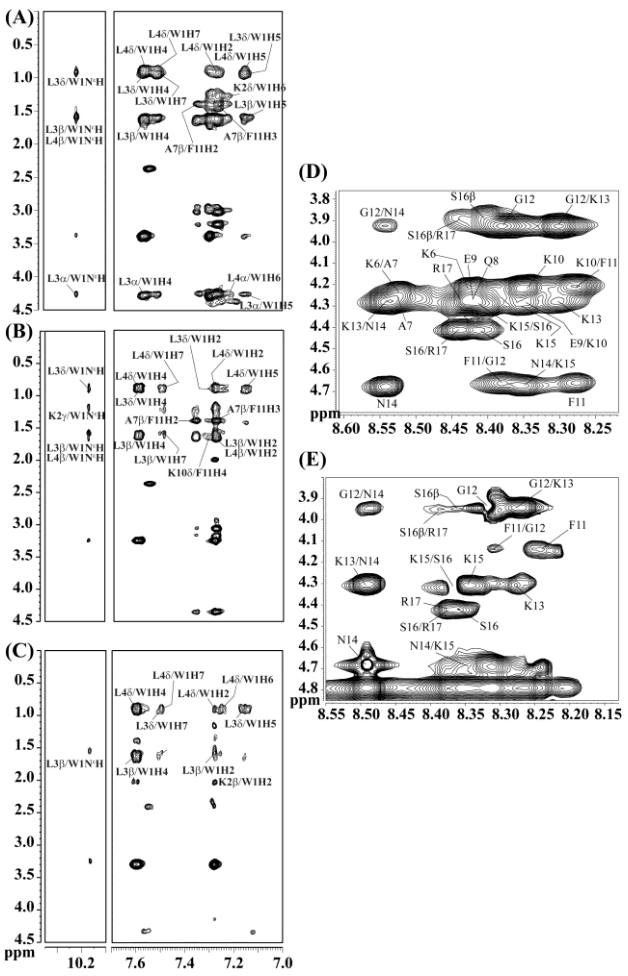

Fig. 7. Analyses of *tr*NOESY spectra of Peptides in LPS micelle. Selected aromatic region of two dimensional ^{1}H-^{1}H *tr*NOESY spectrum of WR17 (A) WG12 (B) and WK10 (C) showing aromatic ring proton connectivities of Trp1 and Phe11 with aliphatic side chain of Leu3/Leu4 and Ala7 depicting close proximity between those residues in the presence of LPS. Fingerprint region of two-dimensional ^{1}H-^{1}H NOESY spectra of KR12 (D) and KR8 (E) in presence of LPS. *tr*NOESY experiments were carried out at 500 MHz and 298 K, with a mixing time of 150 ms.

adopts a conformation that is different from that of the free peptide, giving rise to unique intra-molecular NOE patterns.[39] Due to the chemical exchange at a fast to intermediate time scale happening between the free and the bound form, the bound peptide when released from its binding site, retains its bound conformation for a particular time period, giving rise to intra-molecular constraints of the bound form. As a result, the measured *transferred* NOE (*tr*NOE) can be used to determine the three-dimensional structure of the ligand in the bound state[40, 41]. In general, intermolecular *tr*NOE between the ligand and the LPS could not be detected due to significantly lower concentration of LPS being used for the experiment. In addition to the sequential αN(i, i+1) *tr*NOEs obtained for the peptides, we could also see a large number of medium range *tr*NOEs of the type αN(i, i+3/i+4) in presence of LPS. The aromatic ring protons of Trp1 showed an ample number of *tr*NOEs with the side chains of neighboring aliphatic amino acids such as Leu3 and Leu4 (Fig. 7). The side chain of Ala7 also showed *tr*NOEs with the aromatic ring protons of Phe11 (Fig. 7). Furthermore, the indole ring protons ($N^{\varepsilon}H$) of Trp1 are found to make additional contacts with the adjacent residues of WR17 (Fig. 7). The medium range *tr*NOEs αN(i, i+3/i+4) for WR17 were unambiguously identified between the residues from Trp1 to Phe11, suggesting that the N-ter part of the peptide adopts a helical conformation in the presence of LPS (Fig. 8A and D). Apart from this, several short range *tr*NOEs αN(i, i+2) were also observed for WR17 (Fig. 8A and D). The presence of Gly at the 12th position breaks the helix due to which the C-ter region remains unstructured. WG12 showed almost similar *tr*NOEs to that of WR17 (Fig. 7). All the amino acid residues of WG12 showed a short range αN(i, i+2) as well as medium range *tr*NOEs αN(i, i+3/i+4) bound to LPS (Fig. 8). Also, the aromatic ring protons of Phe11 showed *tr*NOEs with the side chain of Ala7 in the case of WR17 and WG12 with LPS (Fig. 7A and B). In contrast, the *tr*NOE of the aromatic ring proton of WK10 to the neighboring side chain protons was much less in comparison to either WR17 or WG12 (Fig. 7C). Only one αN(i, i+4) and five αN(i, i+3) *tr*NOEs was observed for WK10 in LPS (Fig. 8C and F). A close inspection on the NOE distribution per residue indicated that the Trp1-Phe11 of WR17 was well characterized by a large number of *tr*NOE contacts, whereas the C-ter region (G12-R17) of WR17 showed only sequential NOEs (Fig. 8A and D). The pattern of NOE distribution per residue for WG12 was almost similar to that of the N-ter region of WR17 (Fig. 8). Overall the NOE distribution per residue for WK10 was much less in comparison to either WR17 or WG12. Especially, the medium range NOEs at the C-ter region of WK10 was negligible in the presence of LPS, indicating the C-ter region of WK10 may not be structurally defined. It is noteworthy to mention that neither KR12 nor KR8 in the presence of LPS exhibited any detectable medium range *tr*NOEs αN(i, i+3/i+4) except for a few short range *tr*NOE αN(i, i+2) between Gly12-Asn14 (Fig. 7D-E). The spectrum analysis for the peptides KG11 or KK9 in LPS micelle could not be determined due to severe signal overlap (ESI Fig. S2).

Three-dimensional structure of Peptides bound to LPS Micelle

The three-dimensional structure of the peptides, WR17, WG12, WK10 and KR8 in LPS micelle were determined solely based on the distance constraints obtained from the *tr*NOESY experiments. The superposition of the backbone atoms (N, C^{α} and C′) for an ensemble of 20 lowest energy structures of WR17, WG12, WK10 and KR8 were shown in Fig. 9 (upper panel). The average backbone RMSD values of WR17, WG12, WK10 and KR8 peptides were 1.43 ± 0.53, 0.1 ± 0.05, 0.34 ± 0.13 and 1.06 ± 0.25 Å, respectively (Table S4). The helical conformation of WR17 was found to be disrupted at the residues Phe11-Gly12 due to the non-helical backbone dihedral angle of Gly (Fig. 9). The role of Gly as a helix breaker has been known for a long time.[36, 40] We could not detect any long

range *tr*NOEs between the N-ter helical segment of WR17 and its unstructured C-ter region, suggesting a highly flexibility at C-terminus (Fig. 9). The average backbone RMSD for the residues Trp1-Gly12 is 0.05 ± 0.01 Å for WR17 in the presence of LPS (Table S4). The C-ter region of the peptide is flexible and controlled by the Trp1 residue situated at the beginning of N-terminus. Solution dynamics of WG12 was found to be identical to WR17. Whereas, in WK10, the absence of two residues (Phe11 and Gly12) perturbed the helicity partially, indicating the important role of these residues in maintaining the structural dynamics from randomness to ordered helical conformation. The same observation has been noted for KR12 where Trp1 was completely removed from the sequence (Fig. 9). The crowding of the positively charged residues like Lys and Arg over the entire structure enabled the peptide to interact strongly with the negatively charged phosphate group of LPS. On the other hand, the hydrophobic residues such as Trp1, Leu2, Leu3, Ala7, and Phe11 form a rigid architecture that facilitates the penetration of the LPS membrane (Fig. 9).

Structure of WR17, WG12 and WK10 in presence of LPS is found to be stabilized by the hydrophobic packing between aromatic side chains and the hydrophobic residues of Trp1, Leu3, Leu4, Ala7 and Phe11. The opposite face of the helix is characterized by the charged and the polar residues such as Lys2, Lys6, Glu9 and Lys10. It is to be noted that the Lys6 and Glu9 of the peptides, WR17, WG12 and WK10 form potential salt bridge/hydrogen bond in LPS micelle. However, the unique feature of the structure of WR17 and its N-ter analogues lies within their **$K^2xxxK^6xxxK^{10}$** motifs, which tunes the peptide structure in such a way that the Lys residues can interact with the negatively charged phosphate groups of LPS. Side by side, the interaction between the highly hydrophobic "xxx" tripeptide sequences and the LPS also takes place, resulting in the complete burial of the peptide inside the LPS groove.

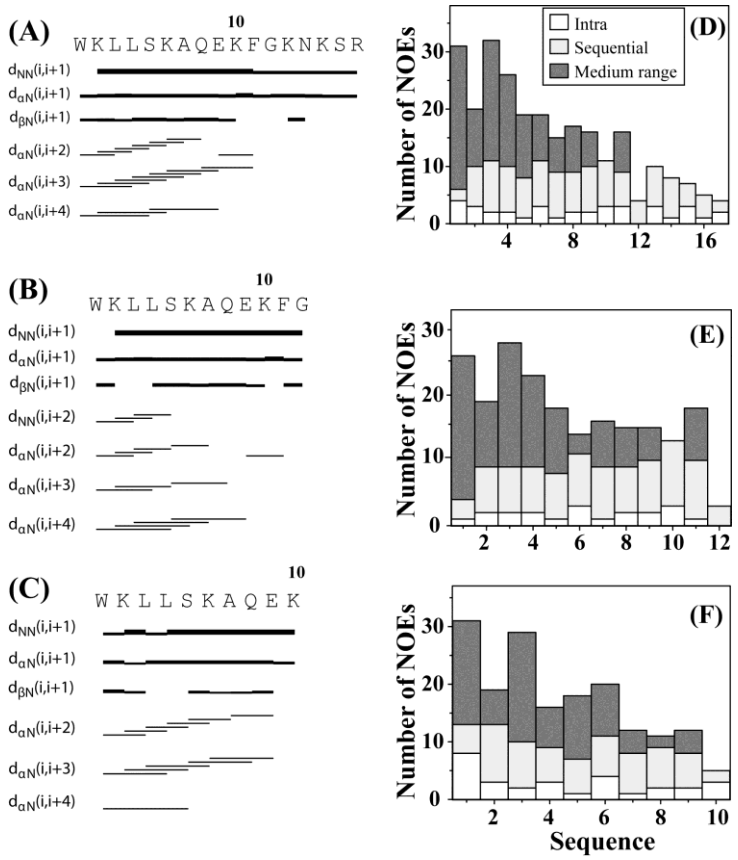

Fig. 8. A summary of NMR structural parameters of peptides in LPS micelle. (Left panel) Bar diagram summarizing type (sequential, medium range, and long-range) and number of NOE contacts, in the *tr*NOESY spectra of WR17 (A), WG12 (B) and WK10 (C) in the presence of LPS among backbone/backbone and backbone/side chain resonances. The thickness of the bars indicates the intensity of the NOESY peaks which are assigned as strong, medium, and weak. The primary amino acid sequences of each peptide are shown at the top. (Right panel) A histogram showing the number and type (intra, sequential, medium) of *tr*NOEs of WR17 (D), WG12 (E), WK10 (F) as a function of residue number in complex with LPS micelle.

Dynamics of Peptides bound to LPS Micelle

Red Edge Excitation Shift (REES) was employed to investigate the dynamics of the environment surrounding the tryptophan residue of WR17 and analogues, in the presence of LPS micelle.[42] REES is well defined by a shift of the emission maximum of fluorophore towards the longer wavelength caused by a shift in the excitation.[43] In viscous or condensed medium the excited state of the polar fluorophore experiences a slow relaxation rate for the solvent manifested as REES. This method can be used to assess biopolymer organization and dynamics in various biochemical systems like ion transport, membrane, micelle, reverse micelle and phospholipid vesicle.[44-46]

A stepwise increment in excitation wavelengths ranging from 280 to 310 nm, does not show any substantial change in the fluorescence emission maxima for WR17, WG12, WK10 in their free states (Fig. 10A-C), suggesting a mobile aqueous environment surrounding the Trp residue. In contrast, when bound to LPS, a significant red shift of 22, 23 and 15 nm in emission maxima of WR17, WG12 and WK10, respectively was observed (Fig. 10A-C). This shows that in the peptide-LPS complex, Trp residues are experiencing an environment where the dynamics of the water molecules have been restricted. This study monitored the presence of the Trp residue at the interfacial region of the LPS micelle, which is characterized by the bulk aqueous phase outside and the hydrophobic membrane environment inside.

Fluorescence anisotropy elucidates the global rotational freedom and the local dynamics surrounding the Trp residues in a protein.[47, 48] This method is very convenient to study the DNA-protein and protein-protein interaction.[47, 49] The effect of the macromolecular size of LPS on a peptide can be well correlated by measuring their anisotropy values. As the free peptides in the solution rotate and tumble rapidly, the rotational diffusion rate will be faster compared to the emission rate of the excited state. Hence, the emitted light will be depolarized to the maximum and the anisotropy will average to zero. Whereas, in LPS, the movement of the peptide will be restricted due to the formation of large molecular weight assembly, which increases the rotational correlation time. This, consequently polarize the emitted light to the extent the anisotropy is present (Fig. 10D-F). Fluorescence anisotropy technique exploits this degree of polarization of the emission, caused by the increase in correlation time of the complex. In our case, the degree of

anisotropy measured, demonstrates the formation of peptide-LPS with longer correlation time depicting the motional restriction of the peptide.

Disaggregation and fragmentation of LPS by the peptides monitored by DLS and ^{31}P NMR

LPS forms soluble aggregates in the aqueous solution due to its inhomogeneous nature. However, the larger aggregated form of LPS with higher molecular weight is more relevant for our study from the biological point of view than its monomeric form.[50] It is noteworthy to mention that the capability of AMPs to lyse the structure of LPS is strongly correlated with the antimicrobial and anti-endotoxin properties of AMPs.[51] Therefore, structural perturbation of LPS micelle by Bovine lactoferrampin and its truncated peptides is examined using Dynamic light scattering and ^{31}P NMR techniques as described below.

Dynamic light scattering (DLS), also known as the photon correlation spectroscopy (PCS), is a technique used to measure the Brownian motion (diffusion) and subsequently the size distribution of an ensemble of particles in the solution. Here, we measured the size distribution of the particle size of free LPS micelles and peptide bound LPS using DLS. It was observed that in the absence of AMPs, LPS micelles had a broad distribution of particle sizes with a hydrodynamic diameter of about ~534 nm (Fig. 11A). The high poly-dispersity of ~72 % suggests that the LPS in free form gets aggregated (Fig. 11A). However, in the presence of WR17 at a molar ratio of 1:1, there is a drastic change in the aggregation pattern of LPS with a reduced hydrodynamic diameter of about ~175 nm (Fig. 11B). In addition, the poly-dispersity also decreased to around ~40 %. Such observations demonstrate that addition of WR17 causes an extensive disaggregation of large LPS micelles into smaller fragments. Similarly, LPS micelle also undergoes structural perturbation in the presence of both WG12 and WK10, with an apparent shift of hydrodynamic diameter to ~200 nm and 230 nm, respectively (Fig. 11C-D). This is also evident from the fact that the poly-dispersity values was reduced to 67 % and 55 % for WG12 and WK10, respectively, suggesting a modest disaggregation of the LPS micelle. In case of KG11, KK9 and KR12, we found a minimal disruption of aggregated state in LPS with negligible change in the polydispersity (Fig. 11E-F). Therefore, these DLS results undoubtedly point towards the fact that disruption of LPS occurs as a result of interaction between native WR17 and its shorter active forms WG12 and WK10 with LPS.

Further, ^{31}P NMR experiment was performed to investigate the plausible interaction between the phosphate groups of LPS with the positive charge amino acid of WR17 or/and its

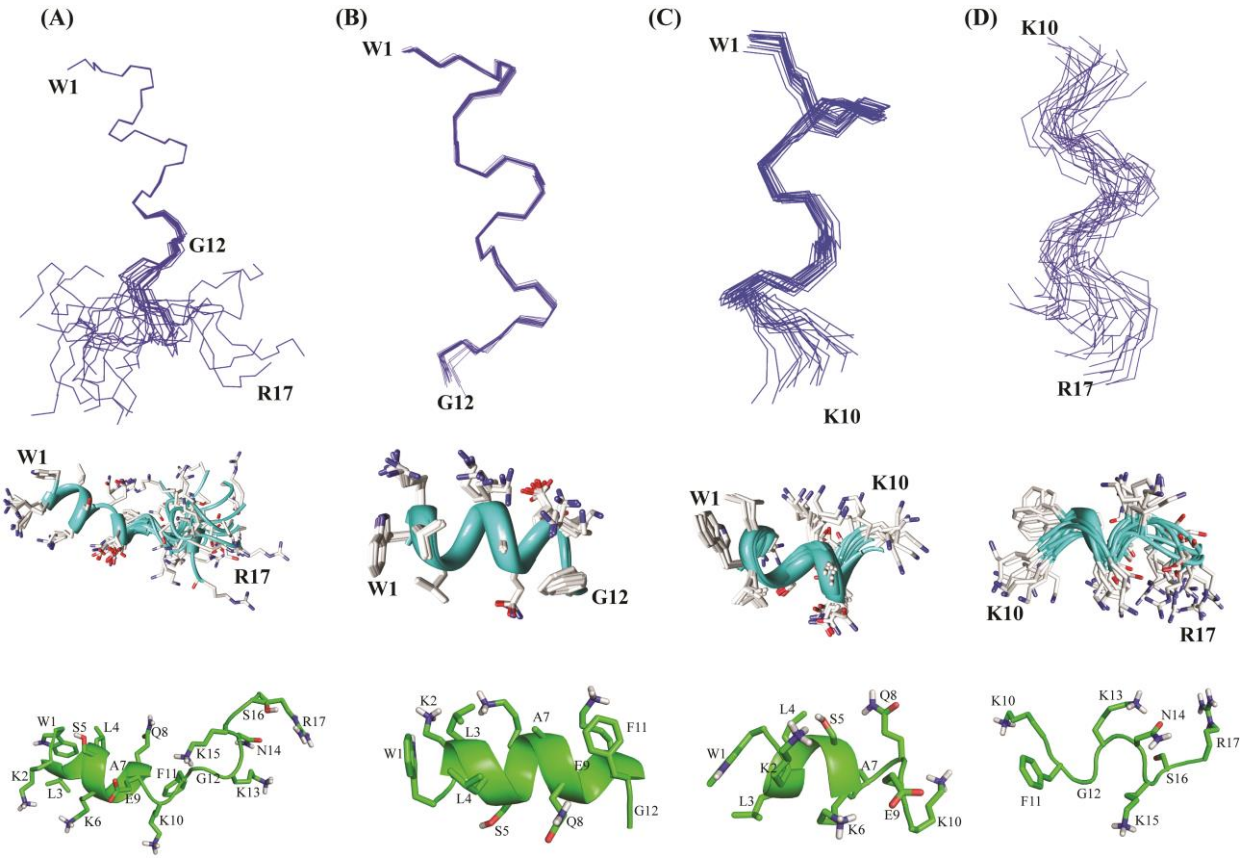

Fig. 9. NMR derived three-dimensional structure of WR17, WG12, and WK10 in LPS micelle. (Upper panel) superposition of backbone atoms (N, C^{α}, and C′) of the twenty lowest energy structures of WR17 (A), WG12 (B), WK10 (C), KR8 (D) bound to LPS micelle, obtained from CYANA 2.1. (Middle panel) Ribbon representative average conformations of WR17 (A), WG12 (B), WK10 (C), and KR8 (D). (Lower panel) cartoon representative conformations of LPS-bound WR17 (A), WG12 (B), WK10 (C), and KR8 (D) showing side-chain positioning and backbone topology. These figures were produced using PyMOL and Chimera.

analogues (Fig. 11G-I). As evident, the addition of WR17 to LPS showed a chemical shift perturbation as well as line broadening of the phosphate groups of LPS. Similar structural perturbation was also observed for the naturally occurring AMPs such as Paradaxin and melittin derived AMPs.[34, 52] However, similar titration of WG12, with LPS showed negligible chemical shift perturbation for phosphate groups of LPS. The C-ter fragment, KR12 was unable to change neither the chemical shift of the phosphate head groups of LPS nor any line broadening was seen. Thus breakdown of large LPS micelle into smaller fragments as found in case of WR17, Such interaction is believed to be crucial for the peptide fragment to initially get attached to the bacterial outer membrane via "$K^{13}NKSR^{17}$", the **molecular anchor** which, subsequently enables the N-ter part of the peptide to penetrate through the outer membrane architecture of gram negative bacteria. Crucial hydrophobic/van-der-Waal interactions were also found between Trp1, Leu3, Leu4, and Ala7 and acyl chain of LPS which in turn is responsible for the activity and stabilization of peptide structure in LPS (Fig. 12A). WG12 was also stabilized by hydrogen bonds and salt bridge interaction with Lipid A part of LPS, in addition to the hydrophobic interactions existing between Trp1, Leu3, Leu 4 and the acyl chain of LPS (ESI Table S1). Interestingly, the lack of "$K^{13}NKSR^{17}$" region in WG12 assisted salt bridge/hydrogen bond formation between Lys2, Lys6 and Lys10 and the phosphate group of Lipid A (Fig. 12B). On the other hand, WK10 orients preferentially in a diagonal manner over the long axis of LPS (Fig. 12C). Two hydrogen bonds were found between the residues Gln8 and Glu9 with LPS, where the former acts as H-bond donor and latter acts as H-bond acceptor with specific functional groups of LPS. Similar to WR17, pronounced hydrophobic interactions were also seen in case of WK10, with the acyl chain of LPS. The shortest fragment KR8, showed strong polar contacts between the phosphate groups of LPS and Lys13, Asn14, Lys15 and Arg17 (Fig. 12D) (ESI Table S1). It is noteworthy that we did not find any crucial hydrophobic interaction between this fragment and LPS. Overall, the docking study agrees well with our experimental results which suggest that the hydrophobic interaction with LPS is crucial for peptide activity.

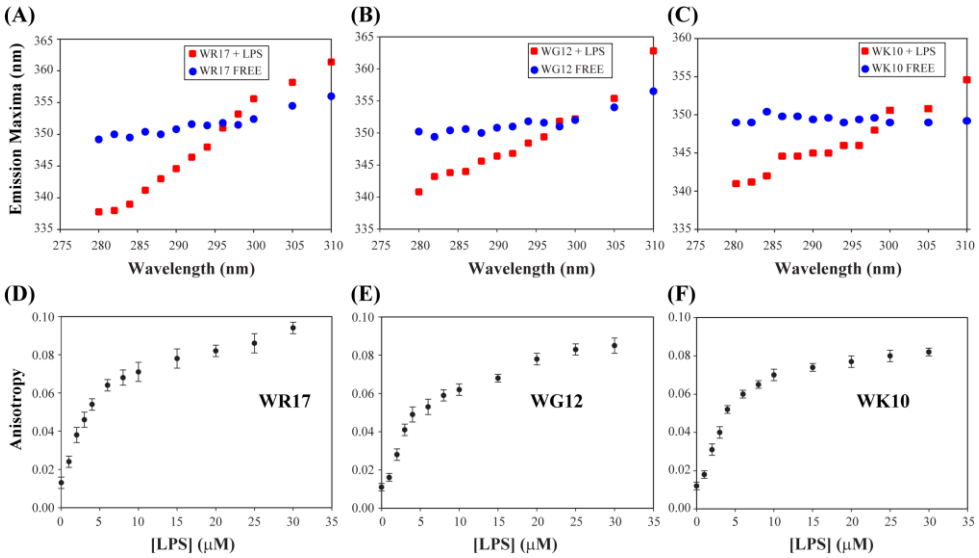

Fig. 10. Probing restricted dynamics of peptides (WR17, WG12 and WK10) in LPS micelle using REES and Fluorescence Anisotropy experiments. The effect of change in excitation wavelengths on the emission maxima of WR17 (A), WG12 (B), WK10 (C) in its free (blue circles) and LPS bound forms (red squares) (Upper panel). A plot showing the change in Anisotropy values of WR17 (D), WG12 (E), and WK10 (F) as a function of concentration of LPS (lower panel).

WG12 and WK10 can be considered to be responsible for the plausible conformational exchange taking place between these two species of LPS at an intermediate time scale (milli second to the microsecond). We can safely exclude the alternate way of interpreting the line-broadening effect, as a consequence of the LPS aggregation, because results from DLS experiments inferred a decrease in the hydrodynamic radius for LPS on addition of WR17.

Docking based interaction analysis of peptides with LPS

Computational molecular modeling was carried out using docking method to understand the structure function relationship by analyzing the arrangement of the key amino acids of the peptide fragments (WR17, WG12, WK10 and KR8) over LPS moiety. Fig. 12 shows the docked conformation of all peptides with respect to LPS. WR17, which is found to be most active peptide from experimental results, showed a unique orientation over LPS with a curvature of 45° in its structural architecture (Fig. 12A). The structured N-ter region of WR17 is aligned diagonally with respect to the long axis of LPS, whereas, the unstructured C-ter end was oriented over Glucosamine I and Glucosamine II of lipid A. Residues such as Lys10, Asn14 and Arg17 are involved in strong hydrogen bonding with the phosphate groups of LPS (ESI Table S1).

MD simulation of WR17 and its fragments with LPS

Tryptophan is one of the key residues, involved in the hydrophobic interaction with acyl chain of LPS. This interaction is quite crucial for the peptide to permeabilize the membrane. Except WR17, this hydrophobic interaction was totally absent for peptides such as WG12 and WK10, where Trp1 was found to be exposed to the exterior solvent throughout the time course of the simulation when simulated in complex with single LPS moiety, as obtained from docking studies. The hydrophobic interaction in WR17 is more pronounced, because Leu3 and Leu4 made crucial contacts being in close proximity to the acyl chains of the LPS. The important feature observed in simulation of WR17 with single LPS moiety is that, the charged residues such as Lys2, Ser5, Lys6 and Lys13 always pointed its side chain towards the solvent, whereas the hydrophobic residues like Trp1, Leu3, Leu4 and Ala7 are buried within the acyl chains of LPS through hydrophobic/van-der-Waal interactions. Overviews of the

motional fluctuations for peptide backbone in association with LPS have been obtained by principal component analysis (PCA) with respect to the first eigenvector (Fig. 13). The relative fluctuations as obtained for WR17 shows porcupines of similar size for the backbone of all residues indicating that the peptide is well stabilized in the presence of LPS. In the case of WG12 and WK10, the C-ter region is more fluctuating compared to the N-ter region of the peptides, suggests that these peptides are relatively less stable in LPS. Solvent accessible surface area (SASA) of the peptides in complex with LPS, calculated from MD simulation also revealed that WR17 when bound to LPS was least perturbed by the solvent. ΔSASA which is calculated as the difference between highest SASA value and that of initial frame of reference shows a value of 38.0 for WR17. In contrast, ΔSASA values for WG12, WK10 and least active peptide KR8 in LPS showed the values of 87.0, 155.3 and 980.8, respectively (ESI Fig. S3). Thus we inferred that there is hardly any hydrophobic interaction between KR8 and LPS. The analysis based on SASA was correlated well with results obtained from REES experiments. Overall, MD simulation provides crucial structural information that can be correlated well with the predicted activity and the experimentally determined NMR structures of WR17 and its analogues.

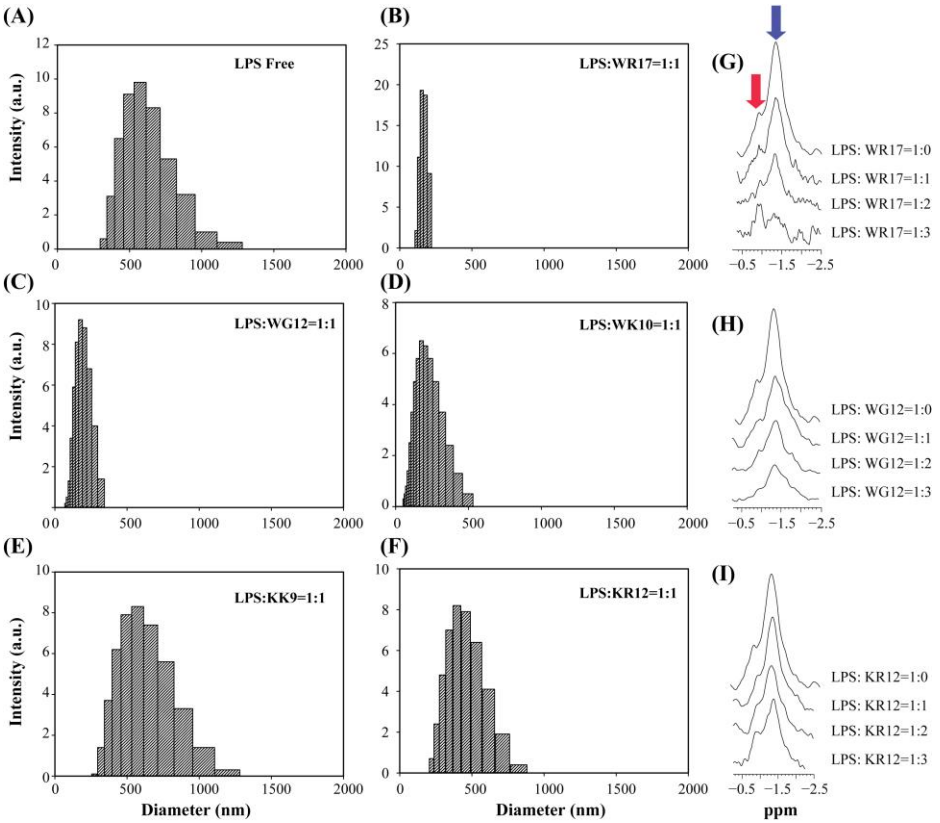

Fig. 11. Structural deformation of LPS micelle by peptides revealed by DLS and ^{31}P-NMR. (Left panel) Bar diagrams showing hydrodynamic diameter (nm) *versus* intensity (A.U) of scattered light for LPS in the absence of peptides (A) and in the presence of peptides, WR17 (B), WG12 (C), WK10 (D), KK9 (E), KR12 (F) at 1:1 molar ratio in 10 mM sodium phosphate buffer (pH 6.0) at 298 K. DLS measurements showed disaggregation of LPS micelle in presence of WR17, WG12 and WK10 from the particle size distribution pattern. (Right panel) Staked plot of one-dimensional ^{31}P-NMR spectrum of 0.5 mM *E. coli* LPS (0111:B4) without peptide and in the presence of different concentrations of WR17 (G), WG12 (H) and KR12 (I) ranging from 0.5 to 1.5 mM. The changes of chemical shift (marked by arrows) as well as the line broadening of ^{31}P resonances of LPS portraying significant structural perturbation of the LPS head group in presence of WR17 and WG12 in contrast to KR12. The NMR experiments were carried out in aqueous solutions (pH 4.5) on a Bruker AVANCE III 500 MHz spectrometer at 298 K.

The role of 'KNKSR' fragment as LPS motif anchoring

The structural information as obtained from NMR derived structure calculation and other biophysical experiments suggests that the bioactive fragment WR17, associates with the LPS micelle, by getting anchored through KNKSR portion. In contrast, the absence of such residues in WG12, WK10 and KR8, has rendered peptides relatively inactive. To better understand the molecular mechanism behind the interaction between the anchor fragment and LPS, we used MD simulations (Fig. 13). The docked pose for WR17 with LPS revealed many key polar contacts, in which, the unstructured C-ter is found to interact only with the GlcN I and GlcN II of lipid A. Residues which are interacting with the negatively charged phosphates such as Lys10 and Arg17 have been shown to maintain the hydrogen bonding throughout the course of the simulation. The terminal residue, Arg17 showed a consistent hydrogen bonding within the range of 2.5-3.1 Å, which highlights the strong nature of this polar interaction (ESI Fig. S4). Based upon the initial anchoring provided by the C-ter part, structured N-ter part is found to establish hydrophobic interaction with the acyl chains of LPS. This interaction is believed to help with subsequent penetration and the disintegration of the micelle (Fig. 14). It is mentioned in the literature that the mechanism of action of WR17 is expected to follow "disordered toroidal".[27] However, as the length of alpha helix is very small either in micelle or in LPS, any model like toroidal pore or barrel Steve can also be expected.

The porcupine plots recounting the relative motions of the backbone atoms with respect to the first prime eigenvector of MD, principal components shows the extreme limits of the fluctuations for all the residues (Fig. 13, left panel). Glycine residue is known to be a helix breaker, which resides at the center of the WR17 sequence divides the fragment into a structured region responsible for the hydrophobic interactions and an unstructured region responsible for the polar interactions. Comparison of the individual RMSF for each of

the atoms suggests a minimal deviation for Gly12 residue, which preserves a 45° degree tilt architecture throughout the course of MD simulation. Similarly, Lys10 also showed a lesser RMSF deviation by forming a hydrogen bond with the phosphate group that ranges in between 1.9-3.0 Å, which brought the fragment in close proximity to the corresponding atoms of LPS (data not shown). As illustrated in the Fig. 13, the fluctuations of each residue is attributed to the combined effect of the interactions with the LPS atoms as well as the nature of the force field used for the simulation.

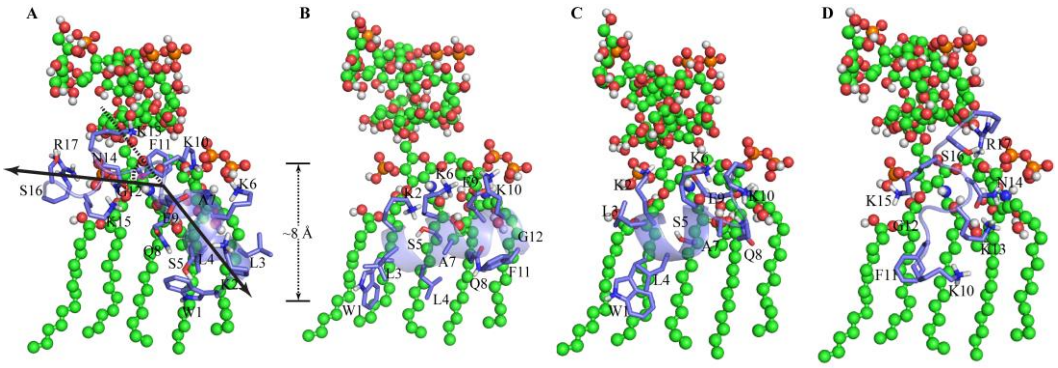

Fig. 12. Docked pose of peptides with LPS. Orientation of (A) WR17, (B) WG12, (C) WK10 and (D) KR8 over LPS moiety. Adaptation of 45° topology of peptide, WR17 to the LPS micelle is highlighted in the figure. An approximate distance of 8 Å was found upon calculation between Trp and lipid A part of LPS. These figures were produced using PyMOL.

Conclusions

The molecular mechanism by which WR17 permeabilizes the membrane and exert potent antimicrobial activity has been addressed in this work in an ad-hoc manner using various biophysical and spectroscopic techniques. The use of fluorescence based biophysical techniques such as calcein leakage, NPN dye uptake and endotoxin neutralization assay could establish that the N-ter region of WR17 is responsible for the membrane permeabilization. With the N-ter and C-ter truncated analogues of WR17 we could further confirm our above hypothesis and found **Trp1** and **Phe11** to be the quintessential residues for stabilization of the N-ter helical structure and activity of WR17. Also with the high resolution NMR structures of WR17 and its analogues, we could identify two unique motif's namely, "$\mathbf{K^2xxxK^6xxxK^{10}}$" and "$\mathbf{A^1xxH^3xxH^6H^7xxxA^{11}}$" which are involved in the polar and hydrophobic interactions with the phosphate group and acyl chain of LPS, respectively. In addition, the MD based simulation suggests that the motif "$K^{13}NKSR^{17}$", present at the C-ter part act as a "**structured molecular anchor"** at the initial stages of the interaction. This anchoring step is necessary for the N-ter helical region to subsequently interact with LPS and permeabilize the outer membrane which in turn is responsible for its antibacterial and endotoxic activity.

Experimental

Reagents

E. coli 0111:B4 LPS was purchased from Sigma-Aldrich Co. (St. Louis, Mo.). Bovine Lactoferrampin (WR17, W268-R284) was purchased from GL Biochem (Shanghai, China) and the shorter fragments, truncated based on sequence of WR17 (scheme 1) were synthesized in Solid phase Peptide synthesizer (Aapptec Endeavor 90) using standard Fmoc chemistry.[53] Synthesized peptides were further purified by reverse phase HPLC system (SHIMADZU, Japan) using Phenomenix C_{18} column (dimension 250 × 10 mm, pore size 100 Å, 5-µm particle size) by linear gradient elution technique using dual solvent system (Water and Acetonitrile) containing 0.1 % TFA. Molecular weight and purity of the peptides were confirmed using MALDI-TOF. Reagents like 4, 4-dimethyl-4-silapentane-1-sulfonic acid (DSS) and deuterium oxide (D_2O) were purchased from Cambridge Isotope Laboratories, Inc. (Tewksbury, MA). All other chemicals and regents were obtained from Acros organics unless specified.

Antimicrobial activity assay

Bacterial cells used for this assay, *e.g.*, *Bacillus subtilis*, *Xanthomonas campestris* and *Pseudomonas aeruginosa* ATCC 27853, were cultured in Muller Hinton (MH) broth at overnight. Overnight cultures were reinoculated and incubated for three hours at 37 °C to obtain log phase culture. Cells were centrifuged and washed twice with the assay buffer (10 mM sodium phosphate buffer, pH 7.4) and diluted to 10^5 cells. 50 µl of the above cell suspensions were incubated for 5 hours at 37 °C, in a sterile 96-well microtiter plate, with an equal volume of peptides at various concentrations, ranging from 1 to 100 µM, diluted from a stock solution of 1 mM (prepared in assay buffer). 200µL MH broth was added to each well and incubated overnight. Absorbance was measured at A_{600}. The minimum inhibitory concentration (MIC) was expressed as the lowest concentration of the peptide where there was no growth of the bacteria.

Calcein leakage assay

This assay was performed according to the protocol published elsewhere.[33] In brief, POPC and POPG were mixed in a molar ratio of 3:1 in 2:1 chloroform/methanol solution to a mass of 20 mg. After that it was lyophilized overnight and hydrated with calcein solution containing 70 mM calcein and 10 mM Tris HCl, pH 7.0 and incubated at 40℃ in water bath for an hour. Next, vortexing the lipid suspension created multilamellar vesicles which were sonicated for three minutes. The vesicle was centrifuged at 14,000 rpm for 10 minutes and extruded through two stacked 50 nm polycarbonate filters for 25 times. Free calcein was removed passing through hydrated Centri Sep spin columns. An iridescent light orange suspension was collected followed by centrifugation at 750 g for 2 min. The

final concentration was of 50 µM in 600 µl of buffer containing 10 mM Tris HCl and 100 mM NaCl, pH 7.4. Fluorescence was measured in a Hitachi F-7000 FL spectrometer in a quartz cuvette having path length of 0.1 cm and bandwidth of 2.5 nm at 25 °C. The excitation and emission maxima were 490 nm and 520 nm, respectively. After stabilization of calcein fluorescence, peptides were added in increasing concentration ranging from 5 µM to 35 µM and a fluorescence intensity increase due to calcein leakage was measured after 5 minutes of incubation. 5 µl of 10 % (v/v) Triton X 100 was used as a positive control to yield the maximum fluorescence intensity or in other words maximum leakage (F_T). Percentage of leakage or SUV permeabilization (P) was measured using the formula as follows:

$P = (F-F_0)/(F_T-F_0) \times 100$……..(Eq. 1)

where, F_0 is the initial basal fluorescence intensity, F is the final fluorescence intensity, 5 minutes after addition of peptide and F_T is the maximal fluorescence intensity after addition of Triton X 100.

NPN dye uptake assay

Midlog phase cells of *E. coli* BL21(DE3) (OD_{600} of 0.5), obtained from an overnight culture of stationary phase cells in LB, were used in this assay. The cells were pelleted by centrifuging at 8000 rpm for 10 min at 25 °C and washed with 10 mM phosphate buffer of pH 7.4 twice and then re-suspended in the same buffer. A hydrophobic dye 1-N-phenylnaphthylamine (NPN) was added to the re-suspended cell with a concentration of 10 µM (prepared in acetone) and was allowed to stabilize for 30 minutes. WR17 and its fragments, WG12, KR12, KG11, WK10 and KK9 were added to cells in increasing concentrations, between 5 µM and 30 µM and the increase in NPN fluorescence, due to permeabilization of the outer membrane was measured on a Hitachi F-7000FL spectrophotometer. NPN fluorescence was measured at an excitation wavelength of 350 nm and a bandwidth of 5 nm and scanning its emission maximum at 410 nm. The baseline fluorescence of the free NPN was subtracted from the total fluorescence for each peptide and percentage increase of NPN fluorescence was calculated in each case, considering Polymyxin B (10 µl of 0.64 µg/ml) to show 100 % increase in NPN fluorescence.[33, 34]

Neutralisation of endotoxin

Neutralization of endotoxin by the designed peptides was estimated using a limulus amoebocyte lysate (LAL) with a Lonza PYROGENT™ Plus kit. The protocol was followed to perform this experiment as per the guidance provided in the kit. Briefly, peptide stocks were prepared in pyrogen-free water given in the kit. 1, 5, 10, 15, and 25 µM peptides were then incubated with endotoxin, in a final volume of 100 µl, at three different concentrations or endotoxin units (EU) of LPS of *E. coli* O55:B5, that were 0.125, 0.25, 0.5, and1EU/ml (1 EU =0.13 ng of LPS) at 37 °C for 30 min to allow peptide binding to LPS.[29] This was next added to an equal volume of lysate and the mixture was further incubated for one hour. Formation of a clot (firm gel) that remains intact momentarily upon inversion of tube characterizes a positive reaction. This suggests the presence of endotoxin and consequently absence of any neutralization. The experiments were repeated thrice, and the average values have been reported.

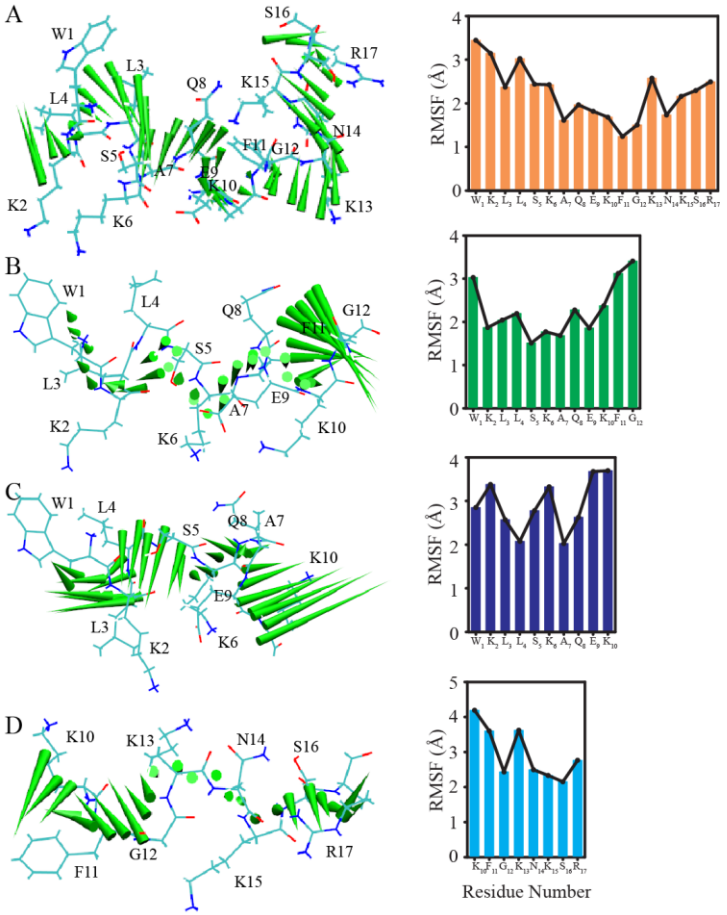

Fig. 13. Molecular Dynamics simulation data. Porcupine plots representing of relative fluctuation of backbone atoms in the simulation time course according to first prime eigenvector (left panel). Residue-wise RMSF have been shown in bar-plot (right panel) for (A) WR17 (B) WG12 and (C) WK10 and (D) KR8.

Fluorescence Spectroscopy

All the fluorescence experiments were performed using Hitachi F-7000 FL spectrometer with a 0.1 cm path length quartz cuvette of at 25 °C. Excitation and emission slit were set to 5 nm. All the peptides and LPS were dissolved in 10 mM Phosphate buffer at pH 6.0. The molecular mass of 10 KDa was considered for *E. coli* 0111:B4 LPS.[39] The intrinsic fluorescence of Trp was used to determine the binding interaction of peptide with LPS using excitation wave length of 280 nm and emission in a range of 300-400 nm. Increasing concentration of LPS (ranging from 0 to 20 µM) was titrated against 5 µM peptides. Binding constant (equilibrium dissociation constant, K_D) of the peptides with LPS were measured by plotting difference in emission maxima as a function of LPS concentration using standard single-site binding curve fitted to equation 2; where, f = fractional saturation of the peptide with respect to LPS expressed in terms of difference in wavelength, $\Delta\lambda_{max} = \lambda_{max}-\lambda(o)_{max}$, λ_{max} =

emission maxima of the peptide on successive addition of LPS in nm, $\lambda(o)_{max}$ = emission maxima of the peptide without addition of LPS in nm, L = ligand (LPS) concentration (μM), K_D = Equilibrium Dissociation constant (μM).

$f = B_{max}.L.(K_D + L)^{-1}$……..... (Eq. 2)

Quenching experiments were performed with free peptides and LPS bound peptides on adding increasing concentration of acryl amide (ranging from 0-0.5 M). Stern-Volmer's constant (K_{sv}) was calculated using the equation 3; where F_0= fluorescence intensity in absence of quencher, F= fluorescence intensity in presence of quencher at each titration, [Q] = concentration of quencher in molarity.

$F_0/F = 1+K_{sv}[Q]$…… (Eq. 3)

Red Edge Excitation Shift (REES) experiment was performed for the free peptide and LPS bound peptide to understand solvent accessibility. The excitation wavelength was varied from 280 to 310 nm and emission profile was monitored in range of 320-400 nm in each case keeping other parameters constant. For each excitation wavelength the emission maxima was plotted for free peptide and LPS bound peptide.

Steady-state anisotropy was recorded with a Hitachi model F-7000 FL spectrometer equipped with a polarized accessory. Anisotropy values were calculated based upon the intrinsic Trp fluorescence property. The fluorescence anisotropy (r) values were obtained using the expression as of Equation 4; where, I_{VV} and I_{VH} are the vertically and horizontally polarized components of probe with excitation by vertically polarized light at 280 nm. G is the sensitivity factor of the instrument. The slits for excitation and emission were set to 5 nm. Each peptide of 5 μM was titrated with increasing concentrations of LPS up to 30 μM.

$r = (I_{VV} - G*I_{VH}) / (I_{VV} + 2*G*I_{VH})$…….....(Eq. 4)

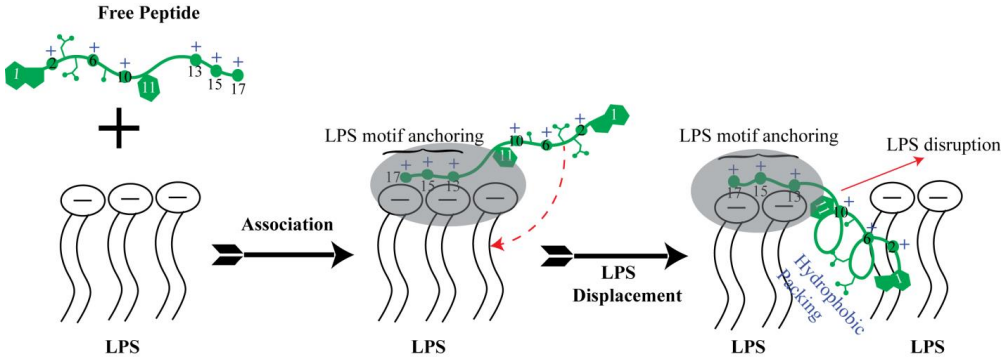

Fig. 14. Schematic representation of mechanistic insight of LPS disruption by WR17. WR17 adopt a random coil structure in aqueous solution where as in LPS micelle it adopts a partial alpha helical structure. The C-ter "$K^{13}NKSR^{17}$" moiety of WR17 interact with phosphate head group of LPS through electrostatic interaction. Then N-terl hydrophobic part disrupt LPS through hydrophobic packing involving acyl chain of LPS and aromatic amino acid residues of WR17, adopting a helical conformation.

Circular dichromism spectroscopy

The peptide secondary structure was determined using a Jasco J-815 spectrometer. Solutions were prepared using 10 mM phosphate buffer at pH 6.0. CD spectra were recorded at 25 ^oC by titrating the increasing concentration of LPS (25-50 μM) against peptides (25 μM). Spectra were obtained with accumulation of three scans, at a speed of 100 $nm.min^{-1}$ over a range of 190-260 nm, at 1 nm data interval. Quartz cuvette of path length 0.2 cm and 0.5 cm were used. The buffer subtracted spectral data obtained in milli-degrees were converted to molar ellipticity (θ) ($deg.cm^2.dmol^{-1}$), using equation 5; where m_0 is milli-degrees, M is molecular weight ($g.mol^{-1}$), L is path length of cuvette (cm) and C is concentration ($g.L^{-1}$).

Molar ellipticity $(\theta) = m_0M/10\times L\times C$….. (Eq. 5)

Measurement of Depth of Insertion of the Peptides into LPS Vesicles by spin labelled lipids

LPS bilayer vesicles (LUVs) were prepared and characterized as described elsewhere.[54] Approximately 5 mg of *E.coli* 0111:B4 LPS was dissolved in 2:1 (v/v) chloroform/methanol solution and it was dried under nitrogen atmosphere. Trace of organic solvent was evaporated to dryness under vacuum pump. After that the lipid film was hydrated with 10 mM phosphate buffer (pH 6.0) at 60 °C in a water bath and vortexed repeatedly for 30 minutes. Next, the lipid suspension was immersed in liquid nitrogen followed by water in a water bath at 60 ^0C for 10 cycles and extruded through a 0.1 μM membrane with the extruder (Avanti Polar Lipids, Alabaster, AL) for 10 times. 5-DSA (shallow quencher) and 16-DSA (deep quencher) stock solutions were prepared in methanol solution and subsequently added to the solution containing 5 μM WR17 and WG12 with 40 μM LPS vesicles. The location of Tryptophan in the LPS bilayer (Z_{cf}) was determined from the following equation using Parallax analysis method.

$Z_{cf}=L_{c1}+[(-1/\pi Cln(F_1/F_2)-L_{21}^2]/2L_{21}$……(Eq. 6)

Where L_{c1} is the difference in depth between the shallow quencher and the bilayer center, F_1 and F_2 are the relative Trp fluorescence intensities in the presence of the shallow and deeper quencher, respectively, L_{21} is the difference in depth between the shallow and deeper quencher, C is the mole fraction of quencher per unit area assuming the surface area of the LPS bilayer to be 70 Å.[55]

Isothermal Titration Calorimetry (ITC)

ITC was carried out to determine thermodynamics of binding of peptides (WR17, WG12, and KK9) with LPS using VP-ITC micro-calorimeter (MicroCal Inc., Northampton, MA). All peptides and LPS were dissolved in 10 mM phosphate buffer at pH 6.0 and degassed. A sample cell containing (volume ~1.5 ml) 10 μM LPS was titrated against peptides from a stock solution of 250 μM at 298 K. A total of 35 injections were carried out at an interval of 4 minutes with 5 μL of peptides aliquots per injection. The raw data was plotted using Micro Cal Origin 5.0 software supplied with the instrument. A single site binding model was used to analysis the association constant (K_A), change in heat of enthalpy of reaction (ΔH), free energy of binding (ΔG) and entropy (ΔS) were evaluated using the equations ΔG = -RT ln K_A and ΔG=ΔH-TΔS, respectively.

Dynamic Light Scattering (DLS)

DLS experiments were performed using Malvern Zetasizer Nano S (Malvern Instruments, UK) furnished with a 4-mW He-Ne laser (λ= 633 nm) and 173° back scattering angle. 1 μM LPS and LPS and peptide at a molar ratio of 1:1 were prepared in 10 mM sodium phosphate (pH 6.0). All samples were filtered using 0.45-μM filter papers (Whatman Inc) and degassed before use and measured at 298 K using low volume disposable sizing cuvette. The viscosity (0.8924) and refractive index (1.330) of 10 mM sodium phosphate buffer were used for data analysis.

NMR experiments

All NMR spectra were recorded at 288 K and/or 298 K with Bruker AVANCE III 500 MHz NMR spectrometer, equipped with a 5 mm SMART probe. Data acquisition and data processing were carried out using Topspin™ *v3.1* software (Bruker Biospin, Switzerland). Two-dimensional total correlation spectroscopy (TOCSY) and nuclear overhauser effect spectroscopy (NOESY) spectra of free peptides and peptide in LPS were acquired in aqueous solution containing 10% D_2O at pH 4.5 with peptide concentration 1 mM. TOCSY mixing time was 80 ms, whereas four different NOESY mixing times, 80, 100, 150 and 200 ms were used for experiments. DSS (2, 2-dimethyl-2-silapentane 5-sulfonate sodium salt) was used as an internal standard (0.0 ppm). Two dimensional *tr*NOESY experiments were performed using 1 mM peptides by titrating various concentrations of LPS ranging from 5 to 25 μM.

A series of one-dimensional proton-decoupled ^{31}P NMR spectra using the Bruker pulse program "zgpg30" were recorded on a Bruker AVANCE III 500 MHz NMR spectrometer to monitor LPS-peptide interactions at 298 K. The ^{31}P NMR spectra of LPS of 0.5 mM concentration were acquired with 3,072 scans. The sample was prepared by dissolving 5 mg LPS in Milli Q water only and pH was adjusted to 4.5. The LPS solution was then titrated with increasing concentrations of WR17, WG12 and KR12.

Calculation of NMR derived structures

All the NMR structures of peptides were calculated by CYANA program *v2.1*.[56] NOE intensities were qualitatively characterized as strong, medium, and weak based upon their respective cross-peak intensities from *tr*NOESY spectra obtained at a mixing time of 150 ms in presence of LPS. This was further translated to inter proton upper-bound distances of 3.0, 4.0 and 5.0 Å respectively. The lower bound distance was kept constant at 2.0 Å. The backbone dihedral angle (phi) was varied from -30^o to -120^o to restrict the conformational space for all residues. No hydrogen bonding constrains were used for structure calculation. Several round of structure refinements were performed and based upon the NOE violations, the distance restraints were adjusted accordingly. The twenty lowest energy structures were selected to generate ensembles of structures of peptides bund to LPS. The structures were analyzed using pymol. The quality of the structures was evaluated using PROCHECK and Protein Structure Validation suite.[57, 58] The calculated peptide structures in presence of LPS were deposited in protein data bank (PDB) with pdb accession codes: 2MD1, 2MD2, 2MD3 and 2MD4 for WR17, WK10, KR8 and WG12, respectively.

Docking calculation of peptides with LPS

Docking calculation of all peptides with LPS was carried out using AutoDock program.[59] Coordinates of LPS were obtained from pdb accession code 1QFG[60] and for peptides (WR17, WG12, WK10 and KR8) the *tr*NOE derived structures were used. Peptides were used as ligand in each docking calculations, with rigid backbone and flexible side chains. A grid spacing of 0.37 Å was used centering the H2 atom of glucosamine II residue of LPS for grid preparation using AutoGrid. All the energy-scoring grids have same size (grid points 70 × 116 × 80) with external grid energy fixed to 1000. Lamarckian genetic algorithm (LGA) was employed as search engine (50 runs) and a LUDI type scoring function.[61] Number of individuals in each population was set to 150. Iteration steps employed for energy evaluation was fixed to 2500,000 and maximum number of generations was fixed to 27,000. The rate of gene mutation and cross over was set to 0.02 and 0.8, respectively. Rest of the parameters used for docking calculations was set as default. Gasteiger-Marsilli charges were used for docking calculations.[62] A charge of +1 value was added to each phosphorus atom to neutralize the system according to Detering and Varani.[63] The generated binding conformations were grouped into clusters based on root-mean-squared tolerance of 1 Å for analysis.

Molecular Dynamics Simulation

Molecular Dynamics (MD) simulation was employed to fetch interaction and binding behavior of peptides in association with LPS. AutoDock generated docked complex of peptide-LPS was employed for MD simulation in explicit solvent (TIP3P water models) conditions. Orthorhombic water box with minimum distance of 10 Å from any heavy atom to box edge was prepared with appropriate number of neutralizing counter ions. MD simulation for 20 ns was performed using Desmond package with OPLS-AA force field.[64] The MD simulation protocol used was similar to that of our previous study.[65] Briefly before the production run, each system was processed for energy minimization and equilibration steps. The energy minimization step was performed in two steps; one with and second without restraints over solute atoms. For equilibration process, each system was first subjected to Berendsen thermostat (NVT ensemble) at 10 K and restraints on solute heavy atoms for 12 ps followed by 12 ps NPT simulation at 10 K with restraints on solute heavy atoms. The temperature was then increased to 300 K and system was simulated for 24 ps with Berendsen NPT ensemble with restraints on solute heavy atoms. A final equilibration step was performed with Berendsen NPT ensemble without any restraints for 24 ps before the production run. A cutoff of 10 Å was used regarding the real-space part of electrostatic and Lennard-Jones interactions. RESPA integrator was used for long-range Coulomb interactions and remaining interactions with time step of 6 fs and 2 fs, respectively. M-SHAKE algorithm was used to constraint the bond-lengths of hydrogen.[66] Trajectories are finally saved at an interval of 2 ps for analysis purpose.

PCA and SASA analysis

The MD simulation trajectory as obtained from Desmond was converted into amber trajectory format using VMD.[67] The trajectory was then compressed for principal component

analysis (PCA) using PCAsuite (http://mmb.pcb.ub.edu/software/pcasuite/). Two program file viz. *pcazip* and *pczdump* was used for preparing average structure for all peptides simulated with LPS. The average structures of all peptides (backbone atoms only) are based on first prime eigenvector. Porcupine plots were prepared to represent the extremes and magnitude of fluctuations for backbone atoms for all peptides interacting with LPS according to the first principal component. Porcupine plots were prepared using a script provided by Neidle group and visualized using VMD program.[68] Calculations of solvent accessible surface area (SASA) have been executed using NACCESS program (http://www.bioinf.manch ester.ac.uk/naccess/). MD snapshots were retrieved at interval of 500 ps and analyzed. ΔSASA have been calculated as difference between highest SASA value and that of 0 ns time snapshot.

Acknowledgements

AB thanks DST FAST track (SR/FT/LS-100/2012) Govt. of India and Institutional start up fund for financial support. SC would like to thank DST, Government of India for Ramanujan Fellowship. AG, AD and JJ thank CSIR, Government of India for fellowship. The Central Instrument Facility (CIF) of Bose Institute is greatly acknowledged for peptide synthesizer, CD, Fluorescence, DLS and NMR instrument facilities. AB thanks Prof. B. Bhattacharyya, Department of Biochemistry, Bose Institute for allowing using the ITC machine and thanks to Mr. Asim K. Poddar for helping in ITC experiment. We thank Professor S. Neidle, University College London, UK for providing the script to generate porcupine plots. Thanks to Dr. K. Janarthan for critical reading of the manuscript. We thank two anonymus referees for their suggestions to improve the quality of the manuscript.

Notes and references

[a]Biomolecular NMR and Drug Design Laboratory, Department of Biophysics, Bose Institute, P-1/12 CIT Scheme VII (M), Kolkata 700054, India.

[b]School of Applied Sciences, Republic Polytechnic, 9 Woodlands Avenue 9, Singapore 738964.

Ψ Authors contributed equally.

To whom correspondence should be addressed: Department of Biophysics, Bose Institute, P-1/12 CIT Scheme VII (M), Kolkata 700054, India, Telephone: +91-33-25693336; Fax: +91-33-23553886; Email: subhro_c@jcbose.ac.in (SC), bhunia@jcbose.ac.in (AB).

† The calculated peptide structures in presence of LPS were deposited in protein data bank (PDB) with pdb accession codes: 2MD1, 2MD2, 2MD3 and 2MD4 for WR17, WK10, KR8 and WG12, respectively.

The abbreviations used are: Antimicrobial peptides, AMPs; NMR, nuclear magnetic resonance; *tr*NOE, *transferred* nuclear Overhauser effect; NOESY, nuclear Overhauser effect spectroscopy; TOCSY, total correlation spectroscopy; NOE, nuclear Overhauser enhancement; LPS, lipopolysaccharide; DLS, Dynamic Light Scattering

*This work was supported by DST FAST track (SR/FT/LS-100/2012) Govt. of India to AB.

Electronic Supplementary Information (ESI) available: [Figures S1-S4 and Table S1]. See DOI: 10.1039/b000000x/

References

1. G. Taubes, *Science (New York, NY)*, 2008, **321**, 356.
2. J. Cohen, *Nature*, 2002, **420**, 885-891.
3. G. S. Martin, D. M. Mannino, S. Eaton and M. Moss, *N. Engl. J. Med.*, 2003, **348**, 1546-1554.
4. E. T. Rietschel and O. Westphal, *Endotoxin in health and disease*, 1999, 1-30.
5. B. Beutler and E. T. Rietschel, *Nat. Rev. Immunol.*, 2003, **3**, 169-176.
6. P. A. Ward, *Nat. Rev. Immunol.*, 2004, **4**, 133-142.
7. S. I. Miller, R. K. Ernst and M. W. Bader, *Nat. Rev. Microbiol.*, 2005, **3**, 36-46.
8. S. Viriyakosol, P. S. Tobias, R. L. Kitchens and T. N. Kirkland, *J. Biol. Chem.*, 2001, **276**, 38044-38051.
9. F. Re and J. L. Strominger, *J. Biol. Chem.*, 2002, **277**, 23427-23432.
10. P. Prohinar, F. Re, R. Widstrom, D. Zhang, A. Teghanemt, J. P. Weiss and T. L. Gioannini, *J. Biol. Chem.*, 2007, **282**, 1010-1017.
11. F. M. Walsh and S. G. Amyes, *Curr. Opin. Microbiol.*, 2004, **7**, 439-444.
12. S. A. David, *J. Mol. Recognit.*, 2001, **14**, 370-387.
13. M. Zasloff, *Nature*, 2002, **415**, 389-395.
14. H. Jenssen, P. Hamill and R. E. Hancock, *Clin. Microbiol. Rev.*, 2006, **19**, 491-511.
15. M. I. van der Kraan, J. Groenink, K. Nazmi, E. C. Veerman, J. G. Bolscher and A. V. Nieuw Amerongen, *Peptides*, 2004, **25**, 177-183.
16. R. E. Hancock and M. G. Scott, *PNAS*, 2000, **97**, 8856-8861.
17. K. A. Brogden, *Nat. Rev. Microbiol.*, 2005, **3**, 238-250.
18. R. E. Hancock, *Lancet Infect. Dis.*, 2001, **1**, 156-164.
19. H. VAN T, I. SIMOONS-SMIT and A. NIEUW, *Biochem. J*, 1997, **326**, 39-45.
20. K. Matsuzaki, *Biochim. Biophys. Acta.*, 1998, **1376**, 391-400.
21. Y. Shai, *Peptide Science*, 2002, **66**, 236-248.
22. E. F. Haney, K. Nazmi, F. Lau, J. G. Bolscher and H. J. Vogel, *Biochimie*, 2009, **91**, 141-154.
23. S. A. Moore, B. F. Anderson, C. R. Groom, M. Haridas and E. N. Baker, *J. Mol. Biol.*, 1997, **274**, 222-236.
24. E. F. Haney, F. Lau and H. J. Vogel, *Biochim. Biophys. Acta.*, 2007, **1768**, 2355-2364.
25. W. C. Wimley and S. H. White, *Nat. Struct. Biol.*, 1996, **3**, 842-848.
26. S. H. White and W. C. Wimley, *B Biochim. Biophys. Acta.*, 1998, **1376**, 339-352.
27. A. Tsutsumi, N. Javkhlantugs, A. Kira, M. Umeyama, I. Kawamura, K. Nishimura, K. Ueda and A. Naito, *Biophys. J.*, 2012, **103**, 1735-1743.
28. E. F. Haney, K. Nazmi, J. G. Bolscher and H. J. Vogel, *Biochim. Biophys. Acta.*, 2012, **1818**, 762-775.
29. D. S. Snyder and T. J. McIntosh, *Biochemistry (Mosc.)*, 2000, **39**, 11777-11787.

30. A. H. Delcour, *Biochimica et Biochim. Biophys. Acta.*, 2009, **1794**, 808-816.
31. P. N. Domadia, A. Bhunia, A. Ramamoorthy and S. Bhattacharjya, *JACS*, 2010, **132**, 18417-18428.
32. A. L. Russell, A. M. Kennedy, A. M. Spuches, D. Venugopal, J. B. Bhonsle and R. P. Hicks, *Chem. Phys. Lipids*, 2010, **163**, 488-497.
33. P. N. Domadia, A. Bhunia, A. Ramamoorthy and S. Bhattacharjya, *JACS*, 2010, **132**, 18417-18428.
34. A. Bhunia, P. N. Domadia, J. Torres, K. J. Hallock, A. Ramamoorthy and S. Bhattacharjya, *J. Biol. Chem.*, 2010, **285**, 3883-3895.
35. S. Bhattacharjya, S. A. David, V. Mathan and P. Balaram, *Biopolymers*, 1997, **41**, 251-265.
36. A. Bhunia, A. Ramamoorthy and S. Bhattacharjya, Chemistry., 2009, **15**, 2036-2040.
37. C. B. Post, *Curr. Opin. Struct. Biol.*, 2003, **13**, 581-588.
38. K. Wuthrich, *NMR of proteins and nucleic acids*, Wiley, 1986.
39. L. Yu, M. Tan, B. Ho, J. L. Ding and T. Wohland, *Anal Chim Acta*, 2006, **556**, 216-225.
40. A. Bhunia, H. Mohanram and S. Bhattacharjya, *Peptide Science*, 2009, **92**, 9-22.
41. A. Bhunia, R. Saravanan, H. Mohanram, M. L. Mangoni and S. Bhattacharjya, *J. Biol. Chem.*, 2011, **286**, 24394-24406.
42. J. R. Lakowicz, *Principles of fluorescence spectroscopy*, Springer, 2009.
43. A. P. Demchenko, *Luminescence*, 2002, **17**, 19-42.
44. A. Chattopadhyay, *Chem. Phys. Lipids*, 2003, **122**, 3-17.
45. A. Chattopadhyay and S. Mukherjee, *Biochemistry (Mosc.)*, 1993, **32**, 3804-3811.
46. A. Chattopadhyay and S. Mukherjee, *J. Phys. Chem B.*, 1999, **103**, 8180-8185.
47. D. M. Jameson and W. H. Sawyer, *Methods Enzymol.*, 1995, **246**, 283-300.
48. J. A. Ross, K. W. Rousslang and L. Brand, *Biochemistry (Mosc.)*, 1981, **20**, 4361-4369.
49. T. Heyduk, Y. Ma, H. Tang and R. H. Ebright, *Methods Enzymol.*, 1996, **274**, 492-503.
50. M. Mueller, B. Lindner, S. Kusumoto, K. Fukase, A. B. Schromm and U. Seydel, *J. Biol. Chem.*, 2004, **279**, 26307-26313.
51. Y. Rosenfeld, H.-G. Sahl and Y. Shai, *Biochemistry (Mosc.)*, 2008, **47**, 6468-6478.
52. A. Bhunia, P. N. Domadia and S. Bhattacharjya, *Biochim. Biophys. Acta.*, 2007, **1768**, 3282-3291.
53. W. C. Chan and P. White, *Fmoc solid phase peptide synthesis: a practical approach*, Oxford University Press on Demand, 2000.
54. A. Bhunia, H. Mohanram, P. N. Domadia, J. Torres and S. Bhattacharjya, *J. Biol. Chem.*, 2009, **284**, 21991-22004.
55. A. Chattopadhyay and E. London, *Biochemistry (Mosc.)*, 1987, **26**, 39-45.
56. P. Güntert, C. Mumenthaler and K. Wüthrich, *J. Mol. Biol.*, 1997, **273**, 283-298.
57. Y. J. Huang, R. Powers and G. T. Montelione, *JACS*, 2005, **127**, 1665-1674.
58. R. A. Laskowski, M. W. MacArthur, D. S. Moss and J. M. Thornton, *J. Appl. Crystallogr.*, 1993, **26**, 283-291.
59. G. M. Morris, R. Huey, W. Lindstrom, M. F. Sanner, R. K. Belew, D. S. Goodsell and A. J. Olson, *J. Comput. Chem.*, 2009, **30**, 2785-2791.
60. A. D Ferguson, W. Welte, E. Hofmann, B. Lindner, O. Holst, J. W. Coulton and K. Diederichs, *Structure*, 2000, **8**, 585-592.
61. H.-J. Böhm, *J. Comput. Aided Mol. Des.*, 1992, **6**, 61-78.
62. J. Gasteiger and M. Marsili, *Tetrahedron Lett.*, 1978, **19**, 3181-3184.
63. C. Detering and G. Varani, *J. Med. Chem.*, 2004, **47**, 4188-4201.
64. *Desmond Molecular Dynamics System, version 2.2 (2009) D.E. Shaw Research, New York, NY. Maestro-Desmond Interoperability Tools, version 2.2, 2009 Schrodinger, New York, NY*.
65. R. K. Kar, P. Suryadevara, J. Jana, A. Bhunia and S. Chatterjee, *J Biomol. Struct. Dyn*, 2013, **31**, 1497-1518.
66. V. Kräutler, W. F. van Gunsteren and P. H. Hünenberger, *J. Comput. Chem.*, 2001, **22**, 501-508.
67. W. Humphrey, A. Dalke and K. Schulten, *J. Mol. Graph.*, 1996, **14**, 33-38.
68. S. Haider, G. N. Parkinson and S. Neidle, *Biophys. J.*, 2008, **95**, 296-311.

Table of Contents

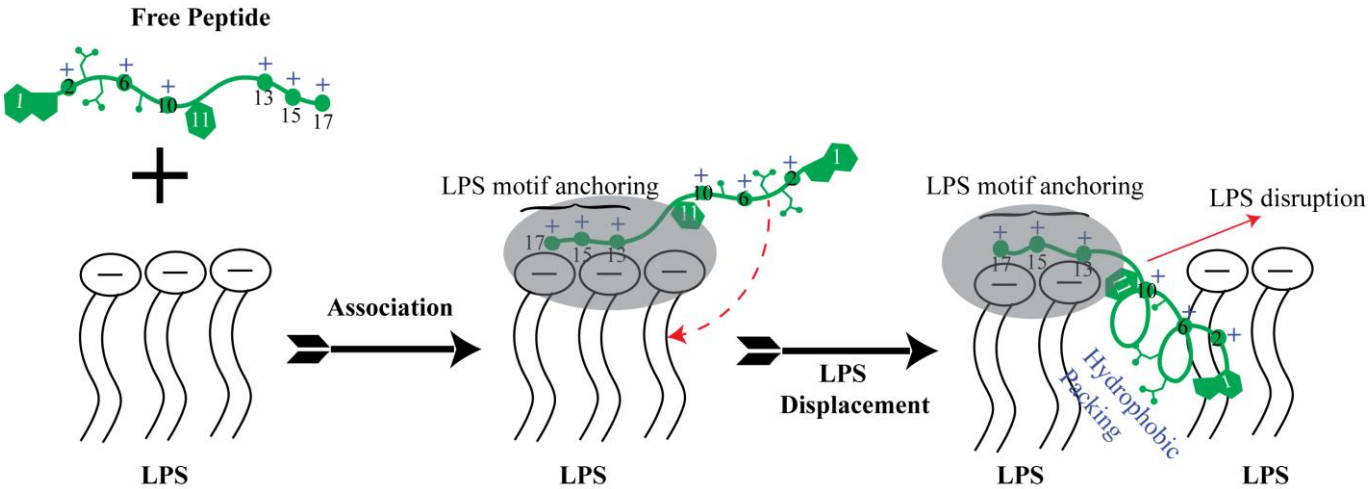

Mechanistic insights of the permeabilization of the outer membrane of gram negative bacteria of an antimicrobial peptide, lactoferrampin, 17 residue peptide using high and low resolution spectroscopy in conjunction with MD simulation.